



HAL
open science

Cyclic High Pressure Torsion of Nickel and Armco Iron

Florian Wetscher, Reinhard Pippan

► **To cite this version:**

Florian Wetscher, Reinhard Pippan. Cyclic High Pressure Torsion of Nickel and Armco Iron. Philosophical Magazine, 2006, 86 (36), pp.5867-5883. 10.1080/14786430600838288 . hal-00513723

HAL Id: hal-00513723

<https://hal.science/hal-00513723>

Submitted on 1 Sep 2010

HAL is a multi-disciplinary open access archive for the deposit and dissemination of scientific research documents, whether they are published or not. The documents may come from teaching and research institutions in France or abroad, or from public or private research centers.

L'archive ouverte pluridisciplinaire **HAL**, est destinée au dépôt et à la diffusion de documents scientifiques de niveau recherche, publiés ou non, émanant des établissements d'enseignement et de recherche français ou étrangers, des laboratoires publics ou privés.



Cyclic High Pressure Torsion of Nickel and Armco Iron

Journal:	<i>Philosophical Magazine & Philosophical Magazine Letters</i>
Manuscript ID:	TPHM-05-Nov-0533.R1
Journal Selection:	Philosophical Magazine
Date Submitted by the Author:	16-Feb-2006
Complete List of Authors:	Wetscher, Florian; Erich Schmid Institute of Materials Science; CD-Laboratory for Local Analysis of Deformation and Fracture Pippan, Reinhard; Erich Schmid Institute of Materials Science; CD-Laboratory of Local Analysis of Deformation and Fracture
Keywords:	deformation, nanostructured materials, cyclic deformation
Keywords (user supplied):	high pressure torsion
<p>Note: The following files were submitted by the author for peer review, but cannot be converted to PDF. You must view these files (e.g. movies) online.</p>	
<p>chptbib.bib</p>	



Cyclic High Pressure Torsion of Nickel and Armco Iron

F. Wetscher^{1,2,*} and R. Pippan^{1,2}

¹Erich Schmid Institute for Materials Science, Austrian Academy of Sciences,
A-8700 Leoben, Austria

²CD-Laboratory for Local Analysis of Deformation and Fracture, Jahnstr. 12,
A-8700 Leoben

Abstract

Cyclic high pressure torsion, a **modified version of high pressure torsion**, is applied to Armco-iron and nickel. The results in terms of microstructure and flow stress are compared to samples deformed by conventional high pressure torsion. For both processes and both materials, a saturation in the decrease of the structure size and the increase in the flow stress is observed. The minimum size of the structural elements which is obtainable is smallest for the conventionally high pressure torsion deformed samples and increases with decreasing strain per cycle in cyclic high pressure torsion.

*Corresponding author. Tel.: +43 3842 804 310; fax: +43 3842 804 116; e-mail: wetscher@unileoben.ac.at

1 Introduction

In the last years numerous papers have proven the capability of the methods of severe plastic deformation (SPD) to produce ultra fine grained and nanograined materials for new applications, see for example [1, 2, 3]. Especially by using equal channel angular pressing (ECAP) with the different routes it is possible to determine the influence of the strain path on grain refinement and the mechanical properties [4, 5]. Nevertheless, the possibilities to vary the strain per pass are very limited and do in most cases comprise a change in the geometry of the tool or the application of composed passes as used in [4]. Furthermore, the total strain reachable by ECAP is limited by practical considerations. The applying of extremely high strains is very time-consuming for the incremental process of ECAP. The simplest method to reach extremely high strains is high pressure torsion (HPT)[6, 7, 8], with the restriction that no change in the strain path can be achieved easily.

Therefore, in this paper a cyclic form of HPT is introduced, cyclic high pressure torsion (CHPT). Due to modifications of our HPT tool it is now possible to cyclically reverse the deformation after a chosen time. The aim of this study is to evaluate the differences between samples deformed by HPT and CHPT in terms of microstructure and mechanical strengths and the influence of the strain per cycle over a wide range of this value.

2 Experimental

The materials used in this study are the bcc Armco iron and the fcc nickel (99.99%). Disks of the materials with an original grain size of approximately $50\mu\text{m}$ were produced with a radius r of 4 mm and a thickness t of 0.8 mm. These disks were deformed by HPT to a total equivalent strain of 64 and CHPT to total equivalent shear strains $\epsilon_{eq,tot}$ of 4, 8, 32 and 64 at a radius $r = 3$ mm.

1
2
3
4
5
6
7
8 The shear strain per cycle $\Delta\epsilon$ was chosen to be 0.5, 1, 2 and 4 at a radius of
9
10 $r = 3$ mm for this investigation. For comparison, samples of nickel with $\Delta\epsilon =$
11 0.5 and 4 and $\epsilon_{eq,tot}=256$ were also examined. The total equivalent shear strain
12 and the strain per cycle are calculated according to Eq. 1 and Eq. 2 where φ is
13 the rotation angle and m is the number of cycles[†].
14
15

$$\Delta\epsilon_{eq} = \frac{\varphi r}{t\sqrt{3}} \quad (1)$$

$$\epsilon_{eq,tot} = m\Delta\epsilon_{eq} \quad (2)$$

16
17
18
19
20
21
22
23 The hydrostatic pressure was kept constant for all experiments at a value of
24 5.7 GPa, the number of turns per minute was 0.2. All deformation experiments
25 were carried out at room temperature, no significant heating of the samples due
26 to the deformation did occur. To evaluate the changes of the flow stress, the
27 torque was measured in-situ by means of strain gauges. From this measured
28 torque, an upper value for the flow stress can be calculated [9, 10]. A sketch of
29 our HPT-tool can be seen in Figure 1. The microstructure was investigated with
30 a Zeiss 1525 scanning electron microscope (SEM) at 20kV using backscattered
31 electrons (BSE). Orientation image maps were measured for nickel samples de-
32 formed with a $\Delta\epsilon$ of 0.5 and 4 by analyzing the Kikuchi patterns caused by
33 back scattered electrons (EBSD). The sample preparation comprised consecu-
34 tive grinding, polishing, etching and a final polishing step. Special care was
35 taken that the samples were not exposed to elevated temperatures during this
36 process to prevent recrystallisation. All micrographs were taken in radial direc-
37 tion as can be seen in Fig. 2.
38
39
40
41
42
43
44
45
46
47

48 [†]one cycle means a deformation in one direction, similar to one pass in ECAP, it corresponds
49 to $\frac{1}{2}$ cycle in conventional fatigue
50
51
52
53
54
55
56
57
58
59
60

3 Results

3.1 Flow stress

A typical measurement of the torque which can be related to the flow stress during CHPT with a $\Delta\epsilon = 1$ of Armco iron as a function of time which is proportional to the accumulated strain is presented in Figure 3a. The negative values of the *flow stress* correspond to an arbitrary definition of a positive and negative direction of the deformation. At the first few cycles, the increase of the flow stress would be almost identical to the flow curve of monotonic deformed samples when absolute values are taken. **In both materials a pronounced work hardening at the first few cycles is present, with an increasing number of cycles the increase of the absolute value of the maximum of the flow stress becomes very low. With higher total strains the cyclic flow curve shows another feature. After changing the strain path, the shear stress at the beginning of the new cycle is markedly lower as the maximum shear stress at the end of the previous cycle and a period with a slow increase of the flow stress is present.** As can be seen in Figure 3b for nickel, this behavior depends on the strain per cycle. It is most pronounced at $\Delta\epsilon = 1$ and 2. After this, a further work hardening occurs with a steep increase of the flow stress until it reaches approximately the same absolute value at the end of the cycle as in the previous one. (Figure 4). It can be seen in Fig. 3b that the slope of this hardening stage decreases with increasing $\Delta\epsilon$. Figure 4a and 4b show the maximum of the flow stresses at each cycle as a function of the total deformation for all applied $\Delta\epsilon$ for Armco iron and nickel, respectively. In both materials the same features are visible. Just like in the monotonic deformed samples, the maximum torque saturates after a certain saturation strain. The lower the $\Delta\epsilon$ is, the lower is also the strain necessary for the onset of this steady state deformation. The quickest saturation can be observed at a $\Delta\epsilon = 0.5$, the highest strain to reach the saturation is necessary

1
2
3
4
5
6
7
8 for the monotonic deformation. It can also be noted for both materials that the
9 higher $\Delta\epsilon$ was, the closer are the curves to the curve for the monotonic deformed
10 samples after the onset of saturation. A difference between the two materials
11 is also the onset strain for the saturation. This strain is higher for the bcc iron
12 compared to the fcc nickel. The maximum torque and therefore the maximum
13 flow stress is slightly higher for Armco iron than for nickel.
14
15
16
17
18

19 3.2 Microstructure

20
21 The resulting microstructures after a deformation to a total strain of $\epsilon_{eq,tot} = 64$
22 for different $\Delta\epsilon$ as can be seen by using backscattered electrons are depicted in
23 Fig. 5 and Fig. 6 for Armco iron and nickel. In all presented micrographs the
24 baseline of the picture is parallel to the shear plane. For both materials the same
25 features are recognizable. The microstructure for the samples with $\Delta\epsilon = 0.5$
26 consists of quite equiaxed elements, the structure size is markedly smaller than
27 $1 \mu\text{m}$, only a weak preferred direction of the elements is detectable. With
28 increasing $\Delta\epsilon$ a decreasing structure size and an aspect ratio of the elements
29 markedly larger than 1 can be observed. Furthermore, a preferred direction
30 of the structural elements is now present. The microstructure of the nickel
31 samples deformed monotonically and the sample deformed with $\Delta\epsilon = 4$ are
32 almost identical. The alignment of the structural elements is naturally in the
33 opposite direction, because the last cycle in the CHPT experiments is always in
34 the 'negative' direction.
35
36
37
38
39
40
41
42
43

44 **In Figure 7, the microstructure of Nickel after monotonic deformation**
45 **to strains of $\epsilon_{eq}=0.5, 1, 2$ and 4 (as large as the strain increments**
46 **in the CHPT experiments) is depicted. After a strain of $\epsilon_{eq} = 0.5$**
47 **the beginning of the formation of a substructure within a grain can**
48 **be seen. When the strain gets larger, more and more well defined**
49 **elements form, until the whole microstructure is very homogeneous,**
50
51
52
53
54
55
56
57
58
59
60

1
2
3
4
5
6
7
8 compare Figure 6e and Figure 7d. During further deformation, the
9 microstructure is still somewhat refined, until this process reaches a
10 steady state.
11

12
13 Figure 8 shows the inverse pole figures calculated from the EBSD measure-
14 ments for different stages of the development of the microstructure for nickel
15 samples deformed with $\Delta\epsilon = 0.5$ and $\Delta\epsilon = 4$. The white lines correspond
16 to boundaries with a misorientation between 2° and 15° , the black lines show
17 boundaries with a misorientation greater than 15° . It can be seen that after a
18 deformation to total strains higher than 16 no significant changes in the struc-
19 ture size occurs. The differences between the samples deformed with $\Delta\epsilon = 0.5$
20 and $\Delta\epsilon = 4$ are similar to those seen in the BSE-micrographs.
21
22

23
24 The evolution of the structural size as well as the ratio of the length of
25 high angle boundaries (HAB) ($\geq 15^\circ$) to low angle boundaries (LAB) (2° - 15°)
26 for nickel is presented in Figure 9. The grain size presented here was evaluated
27 from the EBSD measurements using a misorientation of $\geq 5^\circ$ as a criterion to
28 define a grain boundary. Again, a saturation in the decrease of the structural
29 size can be seen. With increasing total strain, the fraction of the high angle
30 boundaries increases, somewhat faster for the samples with the higher $\Delta\epsilon$. It
31 can be seen that the higher the $\Delta\epsilon$ was, the higher was the fraction of the HAG.
32 The highest value for the fraction of the HAG as well as the smallest structure
33 size was measured for the monotonic deformed sample.
34
35

36
37 In Fig. 10, the misorientation angle distributions of the nickel samples are
38 compared to the random Mackenzie distribution. Only misorientations larger
39 than 5° were taken into account for the calculation of these graphs. Of course,
40 a lot of boundaries with smaller misorientations exists, but they are mainly
41 within the grains. For the samples deformed with $\Delta\epsilon = 0.5$ almost no cor-
42 relation between the misorientation distribution and the random distribution
43 can be seen. For higher total deformations, a slightly higher amount of high
44 angle boundaries is present, but the fraction of small misorientations is still
45
46
47
48
49
50
51
52
53
54
55

1
2
3
4
5
6
7
8 very high. In contradiction to this, the missorientation distribution of samples
9 deformed with $\Delta\epsilon = 4$ converge to the random distribution with increasing total
10 strain. The samples deformed up to $\epsilon_{eq,tot} = 256$ as well as the missorientation
11 distribution of the monotonic deformed sample with $\epsilon_{eq} = 64$ show no further
12 shift to higher missorientation angles.
13
14
15

16 17 18 **4 Discussion** 19

20 The cyclic high pressure torsion can be seen in two contexts. Firstly, as an
21 advancement of the conventional high pressure torsion and also as a similar
22 process like ECAP Route C, and secondly, as a borderline case of fatigue.
23
24
25

26 27 **4.1 Severe Plastic Deformation** 28

29 SPD of pure metals is quite common and therefore a number of papers deal
30 with the evolution of the microstructure and mechanical properties of nickel
31 and pure iron. After HPT, grain sizes in the range of 100 nm to 400nm for
32 nickel are reported in the literature [11, 12, 13, 14]. The grain sizes reported
33 for nickel after ECAP are quite higher, namely between 300nm and 450nm
34 [14, 15, 16, 17]. When comparing such results, one has always to take care
35 that different methods are used to evaluate the grain size. Another important
36 factor is the level of impurities and alloying elements of the used materials [18].
37 Similar results are reported for SPD of pure iron [19, 20, 21]. In the present
38 investigation, the structure size at saturation of nickel was determined from 370
39 nm for the monotonic deformed samples up to 850 nm for the samples deformed
40 with $\Delta\epsilon = 0.5$.
41
42
43
44
45
46
47
48

49 The determination of the structure size as well as the measurement of the flow
50 curve both for nickel and Armco-iron clearly show that in HPT experiments after
51 a total equivalent strain larger than approximately 20 no further refinement of
52 the structure occurs. **This behavior was also shown for pure copper**
53
54
55

1
2
3
4
5
6
7
8 in HPT experiments[9, 22]. A similar saturation in the structure
9 size and in the mechanical strength can also be observed in CHPT
10 experiments, as can be seen in Figure 3 and Figure 8. It can be seen
11 that the strain necessary for the onset of saturation depends on the
12 strain increment $\Delta\epsilon$. The larger $\Delta\epsilon$ is, the larger has to be that onset
13 strain and the more similar is the microstructure of CHPT deformed
14 samples compared to the microstructure of monotonic HPT deformed
15 samples. Hence, an obvious result is that the strain per cycle clearly
16 determines the resulting structure size. Conventional HPT could be
17 compared to ECAP Route A, where there is no rotation of the billet
18 between the passes. Hence, elements are continuously sheared in one
19 direction during multiple passes[23]. CHPT is more comparable to
20 ECAP Route C, where the billet is rotated by 180° along the billet
21 axis. This leads to a forward and backward shearing of an element
22 during successive passes[23]. Therefore, it can be concluded that ECAP
23 Route A will be more effective than Route C in terms of grain refinement,
24 although not necessarily in terms of producing an equiaxed microstructure. This
25 behavior should be well pronounced in most ECAP processes, where a tool angle
26 of 90° is used and the resulting strain per pass is equal to 1. But as can be seen
27 in Fig. 4, the differences at the beginning are not so large as in the steady state
28 regime. This effect of the strain path at ECAP was also found in other studies,
29 for instance in [24, 25]. The conflictive results from other studies [26] may be
30 contributed to the smaller differences at low total strains where the differences
31 are not as significant.

32
33
34
35
36
37
38
39
40
41
42
43
44
45
46
47 In contrast to the saturation in grain size and the mechanical strength, it seems
48 that the ratio between the length of the HAB and LAB as well as the increase
49 in misorientation between neighbouring elements does not saturate as fast as
50 the strength. Hence, one can assume that the mechanical strength is mainly
51 determined by the size of the structural elements and not by the misorientation
52
53
54
55
56
57
58
59
60

1
2
3
4
5
6
7
8 between these elements.

9 *Why does the structure size saturate in HPT and CHPT at different levels?*

10
11 The saturation of the structure size in single phase materials due to severe
12 plastic deformation and its reasons is a topic that is not widely discussed in
13 the literature until recently [22, 27, 28]. It is assumed that processes similar
14 to dynamic recrystallisation or grain boundary sliding are taking place. For a
15 more detailed discussion of this, see [22, 27].

16
17
18
19 **Richert et al.[29] reported that similare stages of deformation are**
20 **observed in cyclic experiments as in experiments with monotonic de-**
21 **formation, although the accumulated strains have to be much higher.**
22 **The reason for this are annihilation processes that are induced by**
23 **the reversal of the shear strain. Stüwe[30] described this behaviour**
24 **mathematical by an efficiency factor η . This factor η describes the**
25 **efficiency to create new dislocations and store them in the structure.**
26 **Only η times the shear strain increment contributes to the increase in**
27 **dislocation density.** There are two limiting cases for η . If $\eta = 0$, no further
28 strain hardening can occur. All dislocations that are created during the de-
29 formation in one direction run backwards and recombine in the former sources
30 during the reversal of the deformation or the number of generated dislocations
31 is equal to the number of annihilated dislocations in one cycle. The other case
32 is that for both directions new dislocations are generated and are stored in the
33 microstructure, therefore η would be equal to 1. If this is true there should be
34 no difference between the cyclic and the monotonic deformation. In Figure 3a
35 it can be seen that this may be the case for the very first few cycles. After a
36 certain number of cycles, the efficiency factor decreases, until after the onset
37 of saturation η is obviously zero over an even number of cycles and no further
38 work hardening occurs. Hence, in this description of the process, the efficiency
39 factor η is itself a function of the total strain and also differs for different $\Delta\epsilon$.
40 It is near one at low total strain and approaches zero as the number of cycles
41
42
43
44
45
46
47
48
49
50
51
52
53
54
55
56
57
58
59
60

1
2
3
4
5
6
7
8 increases. **This efficiency factor can be a useful tool to describe cyclic**
9 **deformation modes, although it has to be noted that no structural**
10 **model is combined with it at the moment.**

11
12
13 But the detailed measurement of the torque show that this description with η
14 is only true when one just looks at the reached maximum values for the torque at
15 the end of the cycle. During the deformation, the torque and therefore the flow
16 stress develops in a different way as described in section 3.1. As can be seen in
17 Fig. 3, after a reversal of the strain path, the torque at the beginning of the cycle
18 is significantly lower than the reached maximum torque after the previous cycle
19 and increases only slightly for a significant fraction of the whole cycle. **This**
20 **region may be the consequence of dislocations running backwards**
21 **toward their sources or newly generated dislocations that annihilate**
22 **with dislocation present on the same slip plane but with different**
23 **sign from the previous cycle. Following this, the flow stress increases**
24 **with a rate that is decreasing with increasing $\Delta\epsilon$. This means that**
25 **after the process of a reversal of dislocation movement or annihilation**
26 **of dislocations is exhausted, new dislocations are created to further**
27 **plastically deform the sample.** For samples with a larger structure size (at
28 the beginning of deformation or small $\Delta\epsilon$) a high work hardening capability exists,
29 therefore the rate of work hardening is large. For the samples with a structure
30 size near the minimum structure size, almost no work hardening capability is
31 left, leading to a slow increase of the flow stress. From the measurement it can be
32 assumed that the flow stress and the structure size of cyclically deformed samples
33 would reach the level of the monotonic deformed samples if the deformation
34 would be carried on monotonic. This behavior can be seen for both materials
35 with the before mentioned difference in the onset of the steady state region.
36
37
38
39
40
41
42
43
44
45
46
47
48
49
50
51
52
53
54
55
56
57
58
59
60

4.2 Fatigue

Of course, it has to be emphasized that the results from CHPT and HPT cannot directly be compared to results from fatigue tests. Nevertheless, many features that are well known in fatigue have similarities with the behaviour of CHPT deformed materials.

Fatigue of nickel and Armco-iron was investigated in many studies, see for example [31, 32, 33, 34, 35]. The presented cyclic hardening curves in these studies show similar characteristics like the measured curves in the present investigation. After an intense hardening stage at the beginning, the stress amplitude saturates in strain-controlled experiments. It is commonly reported [34, 36, 37, 38, 39] that the saturation stress is a function of the plastic strain amplitude for symmetric tension-compression tests both for various single- and polycrystalline materials. The saturation stress increases with the plastic strain amplitude, in some cases a plateau region exists as can be seen in Fig. 11a (from [38]). A question which was not solved till now is: Exists a limit for the cyclic hardening and, if it exists, where is it?

Of course, this can not be easily investigated due to the limit of the plastic strain amplitude in a compression-tension experiment. In the present study, these limits do not exist, although it has to be minded that the deformation mode is different. The increase of the saturation stress (here in terms of the torque) is compared to the monotonic flow curve in Fig. 11b and 11c for Armco-iron and nickel, respectively. For both materials it is obvious that the saturation stress increases with the plastic strain amplitude but the slope of this increase decreases markedly. Finally, for a $\Delta\epsilon = 4$, the saturation stress has about reached the saturation stress for the monotonic deformation mode. The data from conventional fatigue tests would just cover the very left side of the diagrams.

The occurrence of a saturation of the stress in fatigue is generally explained

1
2
3
4
5
6
7
8 by the development of a dislocation network that allows for a further defor-
9 mation without an increase in the dislocation density. The cell size of this
10 dislocation network decreases with increasing plastic strain amplitude and leads
11 therefore to a higher saturation stress according to the mesh-length theory of
12 work hardening [40]. Davidson and Lankford [41] measured the subgrain size
13 in low carbon steels as a function of the cyclic stress range and compared them
14 with results from other studies. A main result is the decrease of the subgrain
15 size with the increasing cyclic stress, the smallest subgrains were found for
16 the monotonic deformation in a tensile test. This is in good agreement with
17 the present results as can be seen in Fig. 9a. The higher the $\Delta\epsilon$ was, the
18 smaller was the structure size in the saturation regime. The smallest structure
19 size was measured for the monotonic deformed sample. The decrease of the
20 structure size for HPT-deformed copper was investigated by Hebesberger et al.
21 [22]. They observed a saturation in the decrease of the structure size at higher
22 strains similar as in the presented experiments in Armco iron and nickel.

23
24
25
26
27
28
29
30
31
32
33 Another feature of conventional fatigue tests is the onset of the saturation in
34 mechanical strength. Generally it is reported that saturation is reached earlier
35 in terms of the number of cycles for larger plastic strain amplitudes. **When for**
36 **example the results from [39] are expressed in terms of the product**
37 **of number of cycles for saturation and the plastic strain amplitude (a**
38 **value comparable to the equivalent strain as calculated in our study),**
39 **the same behavior for fatigue and CHPT is present: The higher the**
40 **strain per cycle, the higher has to be the accumulated strain until**
41 **saturation occurs.** The highest total strain to reach the saturation is needed
42 for the monotonic deformation in HPT.

43
44
45
46
47
48
49 In fatigue experiments, the typical plastic strain amplitudes are quite low
50 (in the order of 10^{-3}) compared to the plastic strains in ECAP Route C or
51 this investigation. Nevertheless, the cell size is comparable or only somewhat
52 larger than the structure size after SPD and the laws governing this size seem to
53
54
55

1
2
3
4
5
6
7
8 be similar. The same characteristics both in terms of structure size and strain
9 hardening are present in both processes. But the much higher stresses that are
10 measured for SPD-deformed materials and now also for the CHPT deformed
11 nickel and Armco iron show that especially the boundaries cannot be directly
12 compared to the structures in fatigued materials. One difference is of course the
13 higher misorientation between the elements in the SPD-deformed materials.
14 But as could be seen in Fig. 10 and Fig. 4, the flow stress is mainly influenced
15 by the structure size and not by the misorientation. Another difference is
16 the high hydrostatic pressure under which SPD takes place. It is assumed [42]
17 that the vacancy concentration is extremely high in these conditions and these
18 vacancies may influence the formation of the boundaries. The boundaries (which
19 are no real grain boundaries) in SPD-deformed materials are sometimes referred
20 as non-equilibrium grain boundaries [6] and seem therefore be a special feature
21 of the very large plastic strains only reached by applying the methods of SPD.
22
23
24
25
26
27
28
29
30
31

32 5 Conclusions

- 33 • Cyclic High Pressure Torsion, a modified version of High Pressure Torsion
34 has been introduced, which permits to easily study many parameters of
35 cyclic severe plastic deformation. The method has been applied to Armco
36 iron and nickel.
- 37 • Monoton deformation by HPT of both material results in a saturation
38 of strain hardening. A similar saturation occurs due to deformation by
39 cyclic high pressure torsion, but the accumulated strain to reach saturation
40 decreases with decreasing $\Delta\epsilon$.
- 41 • The steady state that is reached in terms of mechanical strength is also
42 reached in structure size, the differences in the saturation strength is also
43 reflected in differences of the structure size. The only value that still
44
45
46
47
48
49
50
51
52
53
54
55
56
57
58
59
60

changes somewhat is the misorientation distribution. The higher the total deformation, the more similar is the orientation distribution to the Mackenzie distribution.

- **The structure size strongly depends on the strain increment. The larger the strain increment is, the smaller gets the structure size after the onset of saturation. The smallest structure size was reached for the monotonic deformation by High Pressure Torsion.**

6 References

References

- [1] Y. T. Zhu, T. G. Langdon, R. S. Mishra, S. L. Semiatin, M. J. Saran, and T. C. Lowe, editors. *Ultrafine Grained Materials II*. TMS Publications, Warrendale, Pennsylvania, 2002.
- [2] Y. T. Zhu, T. G. Langdon, R. Z. Valiev, S. L. Semiatin, D. H. Shin, and T. C. Lowe, editors. *Ultrafine Grained Materials III*. TMS Publications, Warrendale, Pennsylvania, 2004.
- [3] M. J. Zehetbauer and R. Z. Valiev, editors. *Nanomaterials by Severe Plastic Deformation*. J. Wiley, VCH Weinheim (Germany), 2002.
- [4] A. Vinogradov, T. Ishida, K. Kitagawa, and V.I. Kopylov. *Acta Mater.*, 53:2181–2192, 2005.
- [5] P. L. Sun, P. W. Kao, and C. P. Chang. In Y. T. Zhu, T. G. Langdon, R. S. Mishra, S. L. Semiatin, M. J. Saran, and T. C. Lowe, editors, *Ul-*

- 1
2
3
4
5
6
7
8 *trafine Grained Materials II*, pages 35–42. TMS Publications, Warrendale,
9 Pennsylvania, 2002.
- 10
11 [6] R. Z. Valiev, R. K. Islamgaliev, and I. V. Alexandrov. *Progr. Mat. Sci.*,
12 45:103–189, 2000.
- 13
14 [7] T. Hebesberger, A. Vorhauer, H. P. Stüwe, and R. Pippan. In M. J. Zehet-
15 bauer and R. Z. Valiev, editors, *Nanomaterials by Severe Plastic Deforma-*
16 *tion*, pages 447–452. J. Wiley, VCH Weinheim (Germany), 2002.
- 17
18 [8] A. Vorhauer and R. Pippan. *Scripta Mater.*, 51:921–925, 2004.
- 19
20 [9] F. Wetscher, A. Vorhauer, and R. Pippan. *Mat. Sci. Eng. A*, in press, 2005.
- 21
22 [10] A. Vorhauer and R. Pippan. *submitted to Acta Mater.*
- 23
24 [11] R. K. Islamgaliev, F. Chmelik, and R. Kuzel. *Mater. Sci. Eng., A*, 237:43–
25 51, 1997.
- 26
27 [12] F. Dalla Torre, P. Spätig, R. Schäublin, and M. Victoria. *Acta Mat*,
28 53:2337–2349, 2005.
- 29
30 [13] E. Schaffler and R. Pippan. *Mat. Sci. Eng.A*, 387-389:799–804, 2004.
- 31
32 [14] A. P. Zhilyaev, B.-K. Kim, J. A. Szpunar, M. D. Baró, and T. G. Langdon.
33 *Mat. Sci. Eng.A*, 391:377–389, 2004.
- 34
35 [15] K. Neishi, Z. Horita, and T. G. Langdon. *Mat. Sci. Eng.A*, 325:54–58,
36 2002.
- 37
38 [16] N. Hansen, X. Huang, and D. A. Hughes. In Y. T. Zhu, T. G. Langdon,
39 R. S. Mishra, S. L. Semiatin, M. J. Saran, and T. C. Lowe, editors, *Ul-*
40 *trafine Grained Materials II*, pages 35–42. TMS Publications, Warrendale,
41 Pennsylvania, 2002.
- 42
43
44
45
46
47
48
49
50
51
52
53
54
55
56
57
58
59
60

- 1
2
3
4
5
6
7
8 [17] N. Krasilnikov, W. Lojkowski, Z. Pakiela, and R. Valiev. *Mat. Sci. Eng.A*,
9 397:330–337, 2005.
10
11 [18] R. Pippan, A. Vorhauer, F. Wetscher, M. Faleschini, M. Hafok, and
12 I. Sabirov. *Mater. Sci. Forum*, 503-504:407–412, 2006.
13
14 [19] R. Z. Valiev, Yu. V. Ivanisenko, E. F. Rauch, and B. Baudelet. *Acta Mat.*,
15 44:4705–4712, 1996.
16
17 [20] Yu. Ivanisenko, A. V. Sergueeva, A. Minkow, R. Z. Valiev, and H.-J. Fecht.
18 In M. J. Zehetbauer and R. Z. Valiev, editors, *Nanomaterials by Severe*
19 *Plastic Deformation*, pages 453–458. J. Wiley, VCH Weinheim (Germany),
20 2002.
21
22 [21] Florian Wetscher, Andreas Vorhauer, Richard Stock, and Reinhard Pippan.
23 *Materials Science and Engineering A*, 387-389:809–816, 2004.
24
25 [22] T. Hebesberger, H. P. Stüwe, A. Vorhauer, F. Wetscher, and R. Pippan.
26 *Acta Mater.*, 53:393–402, 2005.
27
28 [23] M. Furukawa, Y. Iwahashi, Z. Horita, M. Nomoto, and T. G. Langdon.
29 *Mater. Sci. Eng.A*, 257:328–332, 1998.
30
31 [24] A. Gholinia, P. B. Prangnell, and M. V. Markushev. *Acta Mater.*, 48:1115–
32 1130, 2000.
33
34 [25] L. Dupuy and E. F. Rauch. *Mat. Sci. Eng.A*, 337:241–247, 2002.
35
36 [26] T. C. Lowe, Y. T. Zhu, S. I. Semjatin, and D. R. Berg. In T. C. Lowe and
37 R. Z. Valiev, editors, *Investigations and Applications of SPD*, page 237.
38 Kluwer Academic Publishers, Norwell, 2000.
39
40 [27] H. P. Stüwe. *Mater. Sci. Forum*, 503-504:175–178, 2006.
41
42 [28] K. Nakashima, M. Suzuki, Y. Futamura, T. Tsuchiyama, and S. Takaki.
43 *Mater. Sci. Forum*, 503-504:627–632, 2006.
44
45
46
47
48
49
50
51
52
53
54
55
56
57
58
59
60

- 1
2
3
4
5
6
7
8 [29] M. Richert, H. P. Stüwe, M. J. Zehetbauer, J. Richert, R. Pippan, Ch.
9 Motz, and E. Schafler. *Mater. Sci. Eng., A*, 355:180–185, 2003.
10
11 [30] H. P. Stüwe. In M. J. Zehetbauer and R. Z. Valiev, editors, *Nanomateri-*
12 *als by Severe Plastic Deformation*, pages 55–64. J. Wiley, VCH Weinheim
13 (Germany), 2002.
14
15 [31] D.J. Morrison and V. Chopra. *Mater. Sci. Eng., A*, 177:29–42, 1994.
16
17 [32] P. Lukas and L. Kunz. *Mater. Sci. Eng., A*, 189:1–7, 1994.
18
19 [33] C. Buque, J. Bretschneider, A. Schwab, and C. Holste. *Mater. Sci. Eng.,*
20 *A*, 300:254–262, 2001.
21
22 [34] Y. El-Madhoun, A. Mohamed, and M. N. Bassim. *Mater. Sci. Eng., A*,
23 385:140–147, 2004.
24
25 [35] H. Haddou, M. Risbet, G. Marichal, and X. Feaugas. *Mater. Sci. Eng., A*,
26 379:102–111, 2004.
27
28 [36] H. Mughrabi. *Mat. Sci. Eng.*, 33:207–223, 1978.
29
30 [37] A. Giese, A. Styczynski, and Y. Estrin. *Mat. Sci. Eng.A*, 124:L11–L13,
31 1990.
32
33 [38] C. D. Liu, M. N. Bassim, and D. X. You. *Acta metall. mater.*, 42:3695–3704,
34 1994.
35
36 [39] Y. El-Madhoun, A. Mohamed, and M. N. Bassim. *Mat. Sci. Eng.A*,
37 359:220–227, 2003.
38
39 [40] D. Kuhlmann-Wilsdorf. *Metall. Trans.*, 1:3173–3179, 1970.
40
41 [41] D. L. Davidson and J. Lankford. *Int. J. Fracture*, 17:257–275, 1981.
42
43
44
45
46
47
48
49
50
51
52
53
54
55
56
57
58
59
60

- 1
2
3
4
5
6
7
8 [42] M. Zehetbauer, H. P. Stüwe, A. Vorhauer, E. Schafner, and J. Kohout. In
9 M. J. Zehetbauer and R. Z. Valiev, editors, *Nanomaterials by Severe Plastic*
10 *Deformation*, pages 435–446. J. Wiley, VCH Weinheim (Germany), 2002.
11
12
13
14
15
16
17
18
19
20
21
22
23
24
25
26
27
28
29
30
31
32
33
34
35
36
37
38
39
40
41
42
43
44
45
46
47
48
49
50
51
52
53
54
55
56
57
58
59
60

For Peer Review Only

List of Figure Captions

Fig.1 Sketch of the HPT-tool

Fig.2 Sample preparation for microscopy

Fig.3 (a) Measured torque during CHPT experiment, Armco-iron, $\Delta\epsilon = 1$ and during a HPT experiment (b) Details of measured torque curves during CHPT of nickel at different $\Delta\epsilon$, the decrease in the torque after changing the shear direction (+ and -) is indicated.

Fig.4 Measured torque during HPT and the maximum torques in the CHPT experiments (a) for Armco-iron and (b) for nickel

Fig.5 SEM micrographs of Armco-iron taken in radial direction for $\epsilon_{eq,tot} = 64$ at (a) $\Delta\epsilon = 0.5$, (b) $\Delta\epsilon = 1$, (c) $\Delta\epsilon = 2$, (d) $\Delta\epsilon = 4$

Fig.6 SEM micrographs of nickel taken in radial direction for $\epsilon_{eq,tot} = 64$ at (a) $\Delta\epsilon = 0.5$, (b) $\Delta\epsilon = 1$, (c) $\Delta\epsilon = 2$, (d) $\Delta\epsilon = 4$, (e) monotonically deformed

Fig.7 SEM micrographs of nickel deformed by HPT in radial direction for (a) $\epsilon_{eq} = 0.5$, (b) $\epsilon_{eq} = 1$, (c) $\epsilon_{eq} = 2$ and (d) $\epsilon_{eq} = 4$

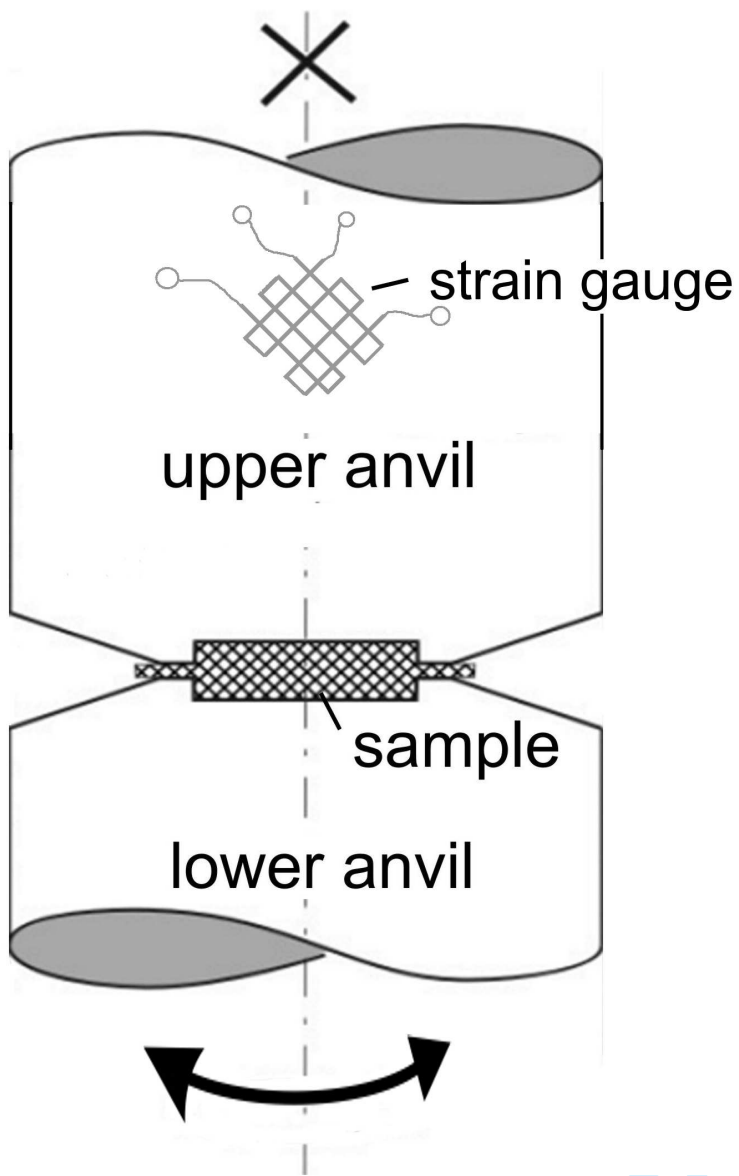
Fig.8 Orientation maps of nickel in axial direction and the standard triangle, (a) $\Delta\epsilon = 0.5; \epsilon_{eq,tot} = 4$, (b) $\Delta\epsilon = 0.5; \epsilon_{eq,tot} = 16$, (c) $\Delta\epsilon = 0.5; \epsilon_{eq,tot} = 64$, (d) $\Delta\epsilon = 4; \epsilon_{eq,tot} = 4$, (e) $\Delta\epsilon = 4; \epsilon_{eq,tot} = 16$, (f) $\Delta\epsilon = 4; \epsilon_{eq,tot} = 64$, (g) $\epsilon_{eq,tot} = 64$, monotonically deformed

Fig.9 (a) Size of the structural elements of nickel as a function of the total equivalent strain (b) ratio between the length of the HAB and the LAB

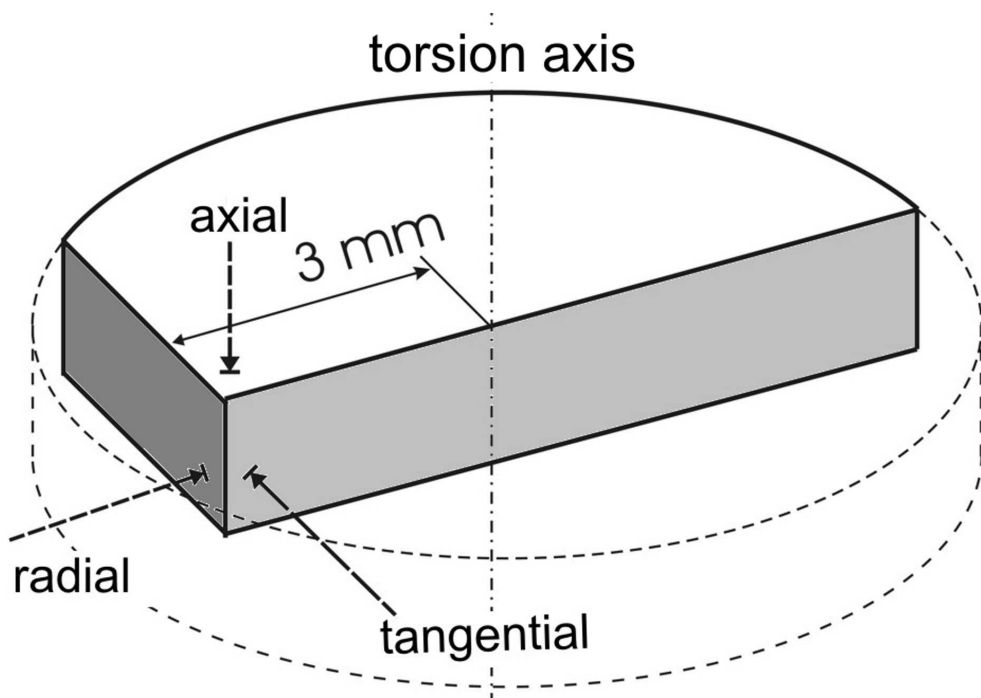
Fig.10 Distribution of the misorientation angle in deformed nickel samples (a) Samples deformed with $\Delta\epsilon = 0.5$ and monotonically deformed sample, $\epsilon_{eq} = 64$ (b) Samples deformed with $\Delta\epsilon = 4$

1
2
3
4
5
6
7
8 Fig.11 (a) Cyclic stress strain curve in fatigued polycrystalline copper [38], (b)
9 Cyclic torque strain curve and the monoton flow curve for iron, (c) Cyclic
10 torque strain curve and the monoton flow curve for nickel ($\Delta\epsilon, \epsilon$ at $r =$
11 $3mm$)
12
13
14
15
16
17
18
19
20
21
22
23
24
25
26
27
28
29
30
31
32
33
34
35
36
37
38
39
40
41
42
43
44
45
46
47
48
49
50
51
52
53
54
55
56
57
58
59
60

1
2
3
4
5
6
7
8
9
10
11
12
13
14
15
16
17
18
19
20
21
22
23
24
25
26
27
28
29
30
31
32
33
34
35
36
37
38
39
40
41
42
43
44
45
46
47
48
49
50
51
52
53
54
55
56
57
58
59
60

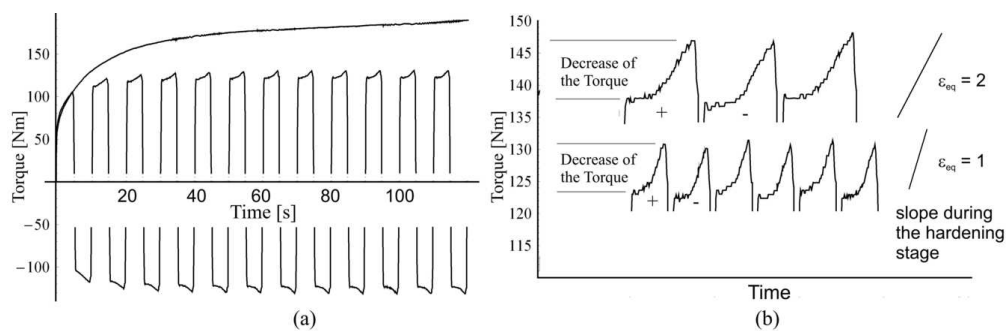


1
2
3
4
5
6
7
8
9
10
11
12
13
14
15
16
17
18
19
20
21
22
23
24
25
26
27
28
29
30
31
32
33
34
35
36
37
38
39
40
41
42
43
44
45
46
47
48
49
50
51
52
53
54
55
56
57
58
59
60



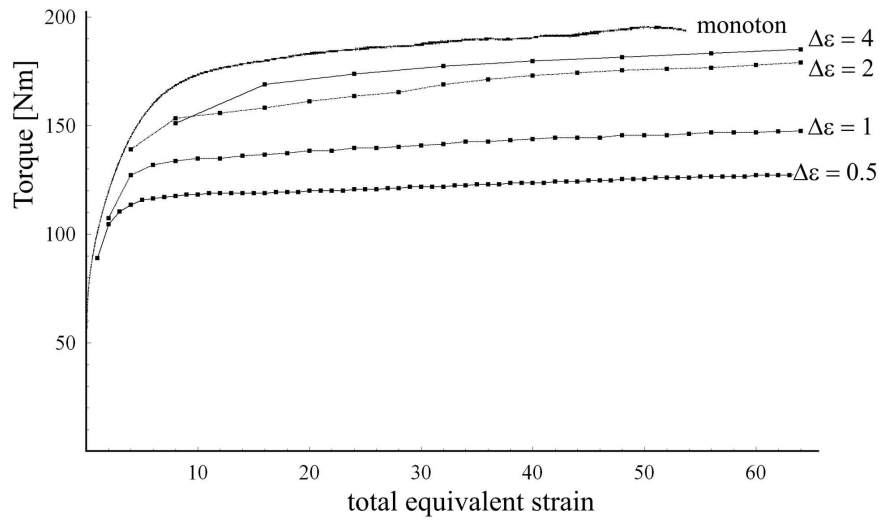
Review Only

1
2
3
4
5
6
7
8
9
10
11
12
13
14
15
16
17
18
19
20
21
22
23
24
25
26
27
28
29
30
31
32
33
34
35
36
37
38
39
40
41
42
43
44
45
46
47
48
49
50
51
52
53
54
55
56
57
58
59
60

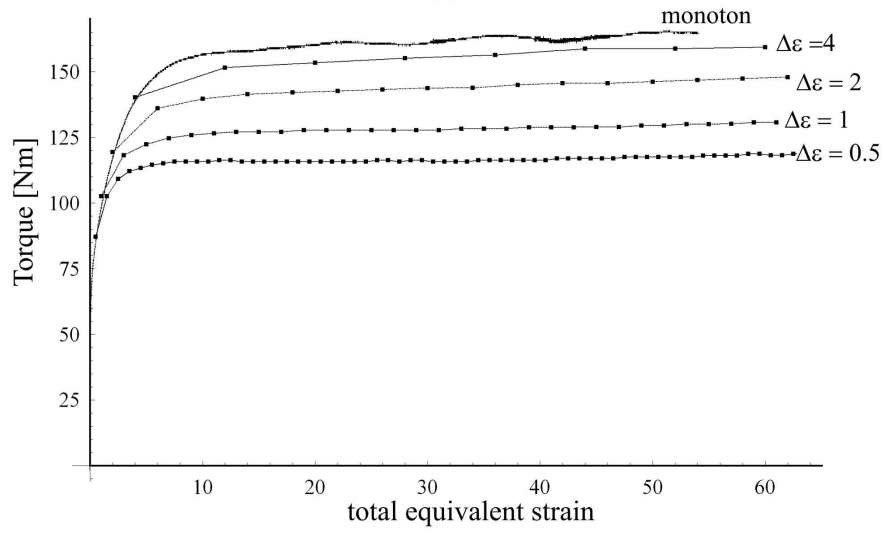


56x17mm (600 x 600 DPI)

Peer Review Only



(a)

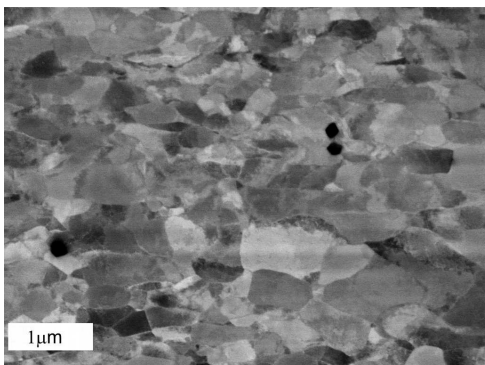


(b)

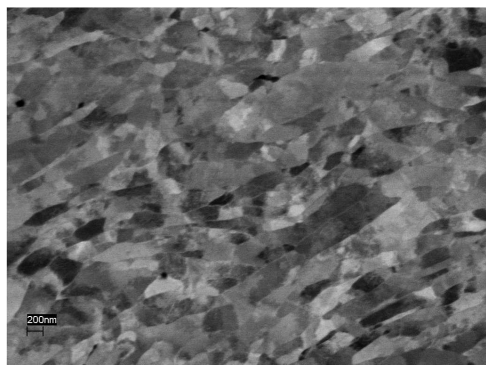
85x113mm (600 x 600 DPI)

1
2
3
4
5
6
7
8
9
10
11
12
13
14
15
16
17
18
19
20
21
22
23
24
25
26
27
28
29
30
31
32
33
34
35
36
37
38
39
40
41
42
43
44
45
46
47
48
49
50
51
52
53
54
55
56
57
58
59
60

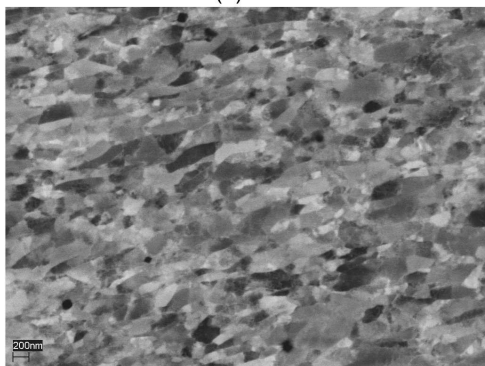
1
2
3
4
5
6
7
8
9
10
11
12
13
14
15
16
17
18
19
20
21
22
23
24
25
26
27
28
29
30
31
32
33
34
35
36
37
38
39
40
41
42
43
44
45
46
47
48
49
50
51
52
53
54
55
56
57
58
59
60



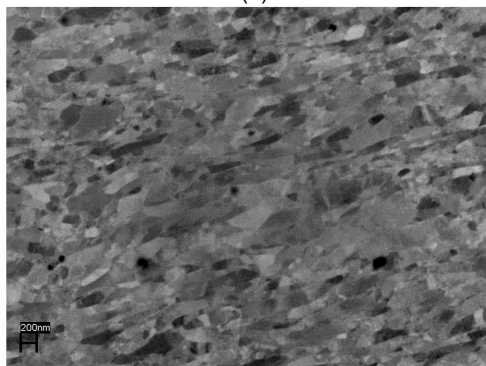
(a)



(b)



(c)

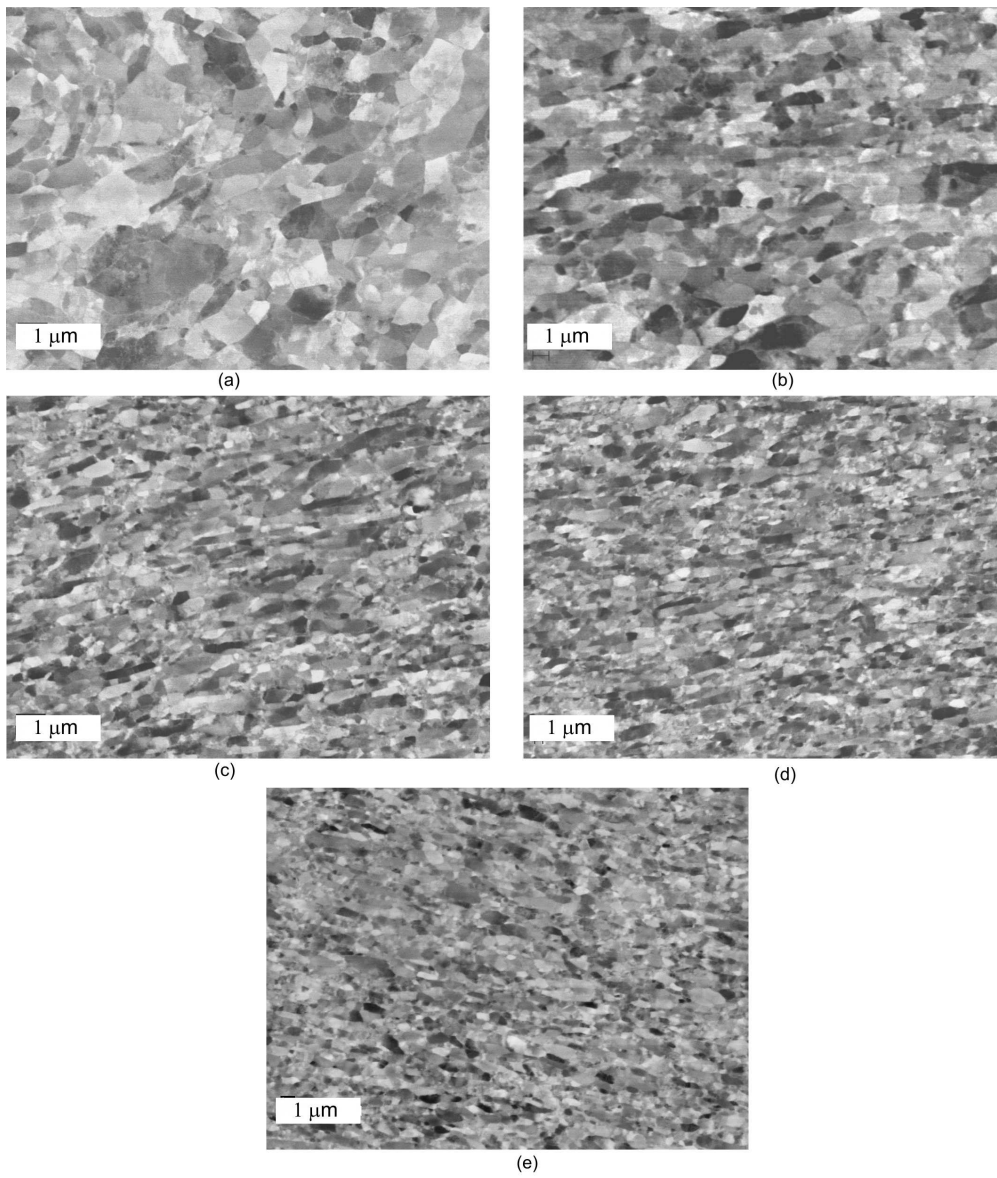


(d)

174x136mm (309 x 309 DPI)

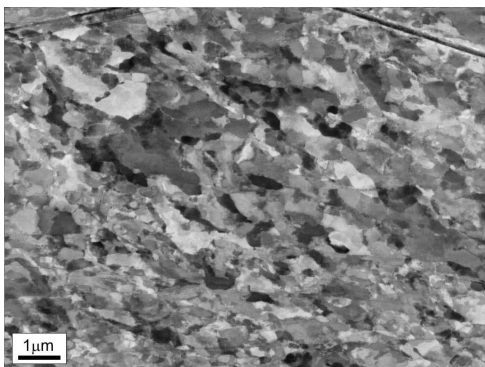
Preview Only

1
2
3
4
5
6
7
8
9
10
11
12
13
14
15
16
17
18
19
20
21
22
23
24
25
26
27
28
29
30
31
32
33
34
35
36
37
38
39
40
41
42
43
44
45
46
47
48
49
50
51
52
53
54
55
56
57
58
59
60

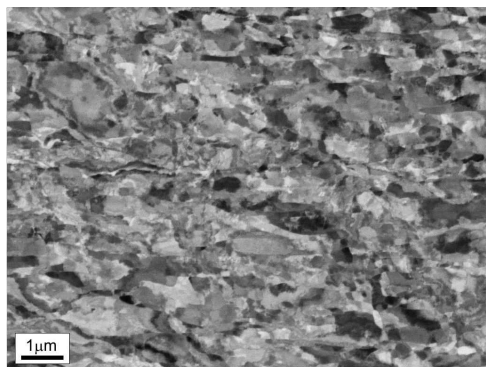


174x204mm (310 x 310 DPI)

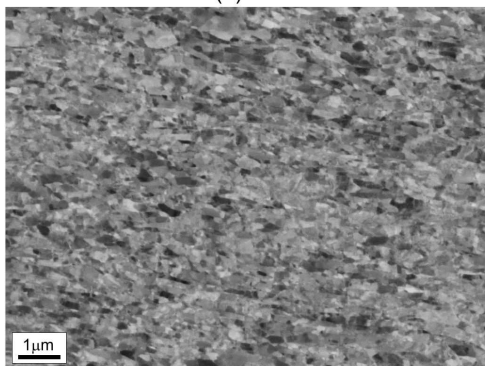
1
2
3
4
5
6
7
8
9
10
11
12
13
14
15
16
17
18
19
20
21
22
23
24
25
26
27
28
29
30
31
32
33
34
35
36
37
38
39
40
41
42
43
44
45
46
47
48
49
50
51
52
53
54
55
56
57
58
59
60



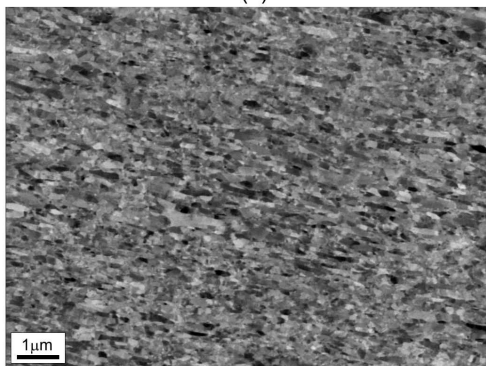
(a)



(b)



(c)

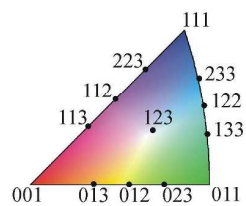
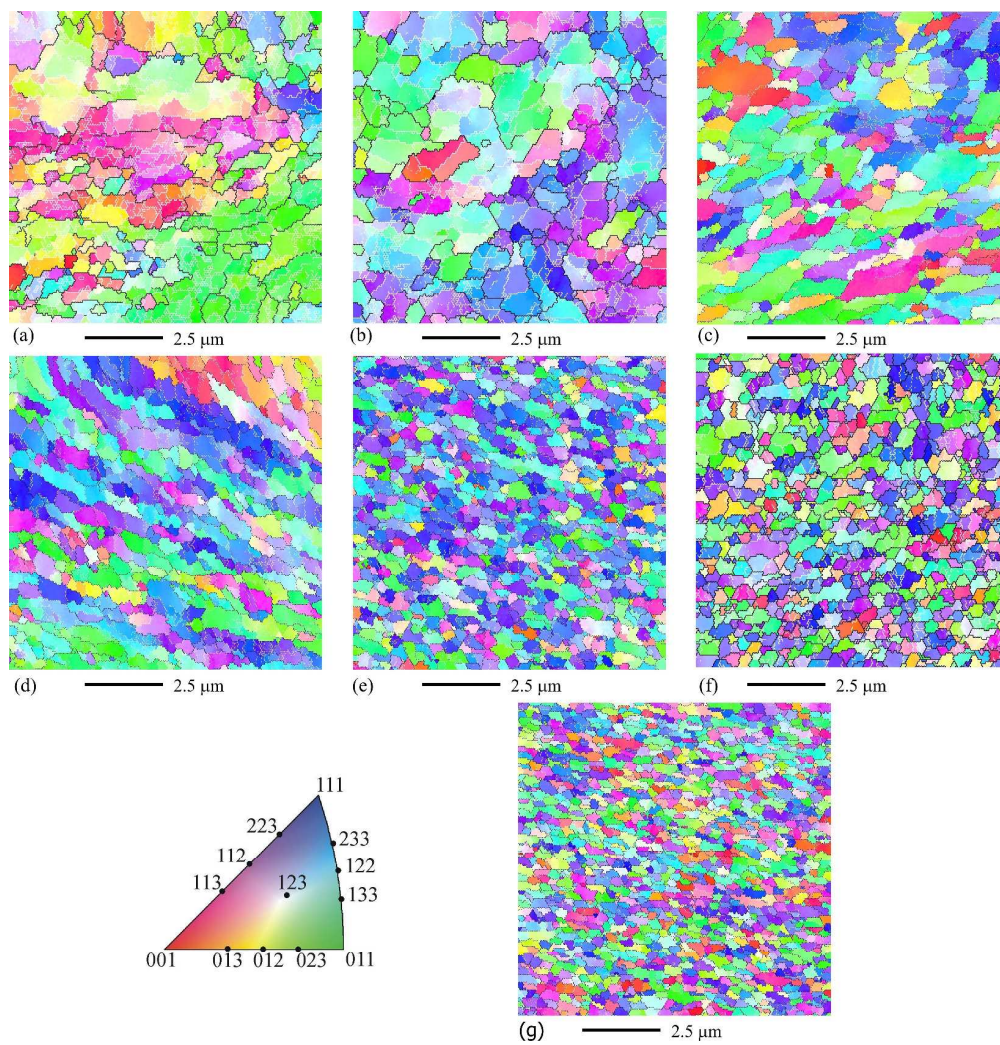


(d)

174x136mm (309 x 309 DPI)

Pre-proof Only

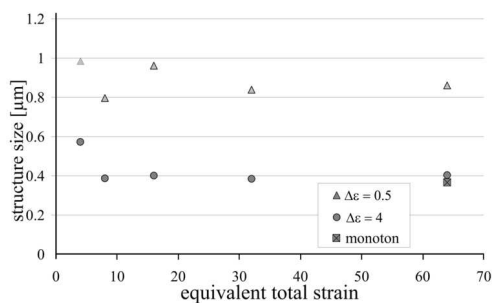
1
2
3
4
5
6
7
8
9
10
11
12
13
14
15
16
17
18
19
20
21
22
23
24
25
26
27
28
29
30
31
32
33
34
35
36
37
38
39
40
41
42
43
44
45
46
47
48
49
50
51
52
53
54
55
56
57
58
59
60



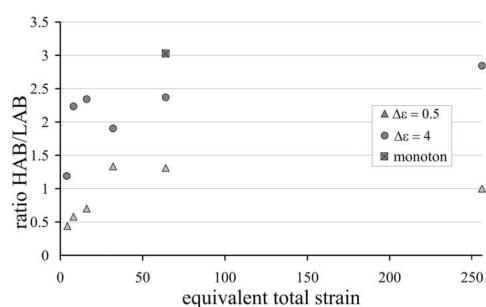
174x180mm (476 x 476 DPI)



1
2
3
4
5
6
7
8
9
10
11
12
13
14
15
16
17
18
19
20
21
22
23
24
25
26
27
28
29
30
31
32
33
34
35
36
37
38
39
40
41
42
43
44
45
46
47
48
49
50
51
52
53
54
55
56
57
58
59
60



(a)

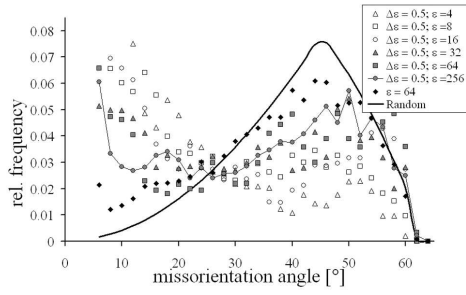


(b)

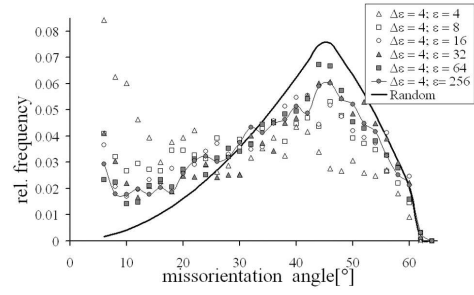
65x24mm (600 x 600 DPI)

Peer Review Only

1
2
3
4
5
6
7
8
9
10
11
12
13
14
15
16
17
18
19
20
21
22
23
24
25
26
27
28
29
30
31
32
33
34
35
36
37
38
39
40
41
42
43
44
45
46
47
48
49
50
51
52
53
54
55
56
57
58
59
60



(a)

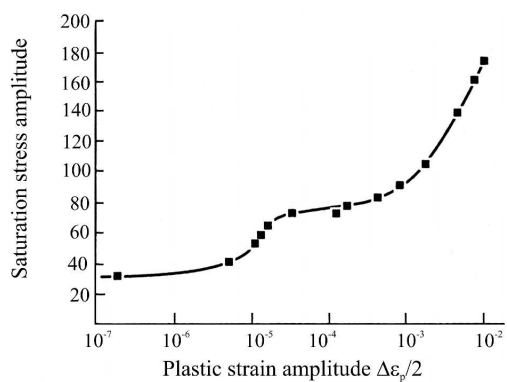


(b)

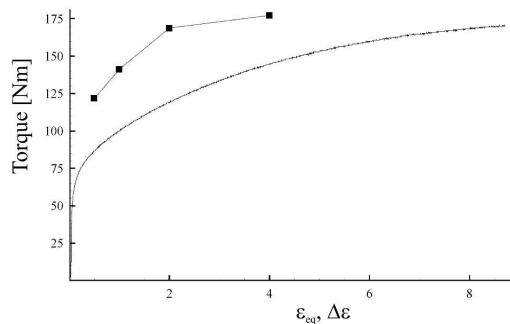
175x59mm (600 x 600 DPI)

Peer Review Only

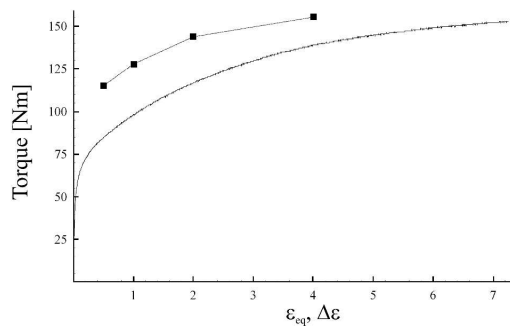
1
2
3
4
5
6
7
8
9
10
11
12
13
14
15
16
17
18
19
20
21
22
23
24
25
26
27
28
29
30
31
32
33
34
35
36
37
38
39
40
41
42
43
44
45
46
47
48
49
50
51
52
53
54
55
56
57
58
59
60



(a)



(b)



(c)

85x190mm (600 x 600 DPI)